AIP Journal of Applied Physics

Temperature-time transformation diagram for Pb(Zr,Ti)O3 thin films

Ronnie Varghese, Matthew Williams, Shashaank Gupta, and Shashank Priya

Citation: Journal of Applied Physics **110**, 014109 (2011); doi: 10.1063/1.3606433
View online: http://dx.doi.org/10.1063/1.3606433
View Table of Contents: http://scitation.aip.org/content/aip/journal/jap/110/1?ver=pdfcov
Published by the AIP Publishing

Temperature-time transformation diagram for $Pb(Zr,Ti)O_3$ thin films

Ronnie Varghese,[1] Matthew Williams,[2] Shashaank Gupta,[1] and Shashank Priya[1,a)]
[1]*Center for Energy Harvesting Materials and Systems (CEHMS), Department of Materials Science and Engineering, Virginia Tech, Blacksburg, Virginia 24061, USA*
[2]*Department of Statistics, Virginia Tech, Blacksburg, Virginia 24061, USA*

(Received 23 February 2011; accepted 28 May 2011; published online 14 July 2011)

In this paper, we describe an analytical model to define the temperature-time- transformation (TTT) diagram of sol-gel deposited $Pb(Zr,Ti)O_3$ thin films on platinized silicon substrates. Texture evolution in film occurred as the pyrolysis and thermal annealing conditions were varied. We demonstrate that the developed model can quantitatively predict the outcome of thermal treatment conditions in terms of texture evolution. Multinomial and multivariate regression techniques were utilized to create the predictor models for TTT data. Further, it was found that multinomial regression can provide better fit as compared to standard regression and multivariate regression. We have generalized this approach so that it can be applied to other thin film deposition techniques and bulk ceramics. © *2011 American Institute of Physics*. [doi:10.1063/1.3606433]

I. INTRODUCTION

$Pb(Zr,Ti)O_3$ (PZT) thin films deposited using sol-gel process, a chemical solution deposition (CSD) technique, are frequently used in micro-electronics industry. This industry focus has lead to detailed studies on the effect of sol-gel process variables on texturing of PZT films. It is well known that piezoelectric properties are maximized along certain crystallographic directions depending upon the parent phase symmetry. To exemplify, <001> oriented single crystals of morphotropic phase boundary composition 0.92 $Pb(Zn_{1/3}Nb_{2/3})O_3$ – $0.08PbTiO_3$ (PZNT) have been shown to possess high electromechanical coupling coefficients of 0.94, high piezoelectric constants of between 2000 and 2500 pC/N and high electrically induced strains of 1.7%.[1–4] Park and Shrout attributed this high electromechanical performance to domain engineered state achieved through polarization rotation from <111> to <001>.[3,4] First principles calculations have indicated that the transformation under electric field between ferroelectric rhombohedral and ferroelectric tetragonal phases proceeds by rotation of the polarization between <111> and <001>, via the <110>.[5] This rotation causes a large coupling between the polarization and electric field causing a giant piezoresponse. In general, a rhombohedral composition oriented along <100> direction and a tetragonal composition oriented along <111> direction will exhibit optimum magnitude of electromechanical coefficients.[6] Thus, texturing is desired in PZT but poses several challenges in synthesis. The growth of bulk PZT in single crystal or textured form has been difficult due to the incongruent melting of ZrO_2. However, PZT films can be textured due to the low annealing temperature required to achieve proper crystallinity. The questions which we pose in this study are as follows: "How to predict the texture of sol-gel deposited PZT thin films with a high degree of confidence?"; and "Can a generalized mathematical model be developed for predicting the texture in ferroelectric materials in terms of synthesis parameters for any given synthesis process?".

There are numerous variables in sol-gel deposition process including a choice of bottom electrode, interfacial layers, precursor chemistry and concentration, solvent, chelating agents, dilution rate (determined by molarity and effects viscosity of sol), hydrolysis ratio, spin coating speed and times, and pyrolysis and annealing conditions (including ramp up and down rates).[7] The innumerability of the variables presents the difficulty in optimizing the conditions for achieving high texture degree. Further, it makes the deposition process susceptible to human errors. This is evident from the fact that a large pool of data exists in literature on sol-gel deposition of PZT thin films but the research has shown that there exists significant variations in the measured results across the laboratories. For repeatability, current methodology requires detailed documentation of process conditions and procedures and access to a similar type of equipment and starting material. The situation becomes more complex when one is looking for specific texture in the deposited film. This describes the motivation behind our study. We focus on developing mathematical criterion for predicting the texture in sol-gel deposited thin films by fixing many of the variables and just varying the pyrolysis and thermal annealing conditions. These two variables are most commonly used to modulate the phase of the films and thus we could refer to them as "texture controlling parameters" (TCP).

In PZT sol-gel studies, temperature-time-transformation (TTT) diagrams have been developed to represent the variation of texture as a function of TCP.[8] These diagrams are commonly invoked to understand the texturing mechanisms[9,10] and quantify the operating regime for achieving specific orientation. However, these diagrams are just pictorial guides specific to a given sol-gel deposition process. Besides, these guides can be misleading as they can only depict the dominant crystalline phase or texture and do not provide the reader with an understanding of the extent of

a)Author to whom correspondence should be addressed. Electronic email: spriya@vt.edu.

the other mixture of phases. Mathematical modeling of the TCP data has never been attempted and therefore, no predictor models are available. This paper attempts to fill that void by proposing a statistical methodology to predict the crystalline orientation. The ability to define the boundaries in terms of TCP will allow repeatability in synthesis of textured films.

Polycrystalline thin films can have one or two predominant crystalline orientation. Compiling X-ray diffraction (XRD) data from several samples can lead to binary trends, that is, higher the texturing in one orientation lower it is in the other possible orientations. In case of PZT 60/40 (where Zr = 0.60 and Ti = 0.40 mole fraction) thin films, the three dominant textures are <100>, <110>, and <111>; and therefore, the data can be considered trinomial and interdependent. Standard multiple regression methods cannot adequately describe these interdependent responses and so multivariate regression is recommended. But multivariate regression approaches can be complicated and difficult. Thus, a non-linear simultaneous or multinomial regression approach is proposed and compared to consecutive multiple and simultaneous multivariate linear regression approaches.

II. EXPERIMENTAL PROCEDURE

The sol-gel deposition process (see Fig. 1) was optimized from that described in Ref. 11 and consists of the following steps: (1) preparation of the sol from Pb, Zr, and Ti precursors in a glovebox; (2) spin coating of the sol onto the substrate; (3) pyrolysis of the sol-gel thin film on a hot plate to remove solvents and organics and; (4) densification and crystallization of the thin film in a high temperature tube furnace. The mixture of individual sols results in a final composition of 0.4M $Pb_{1.1}(Zr_xTi_{1-x})O_3$ with x = 0.6. An extra 10% Pb was included to compensate for the losses during thermal treatments as PbO has high vapor pressure of 2 Torr at 700 °C.

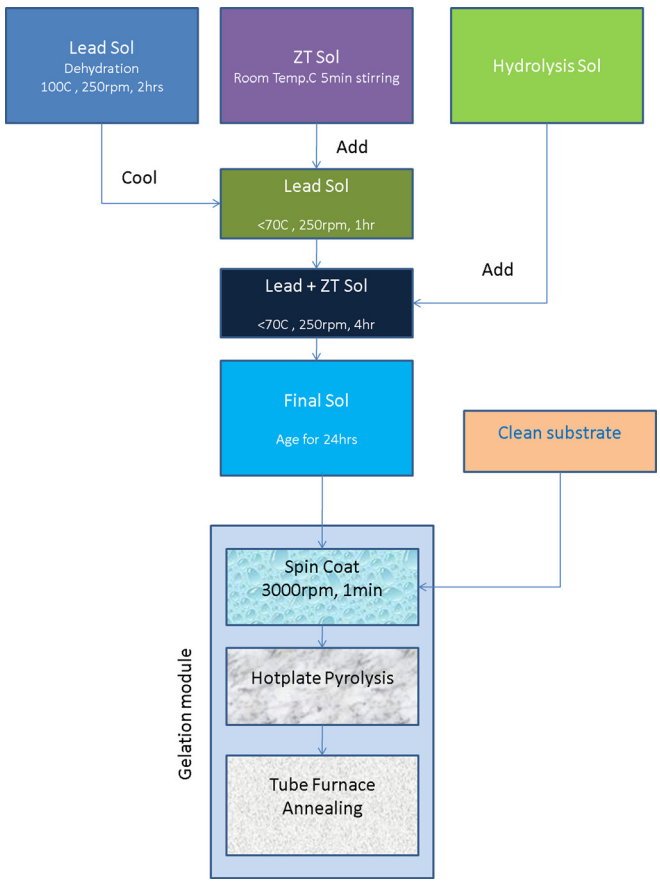

FIG. 1. (Color online) Sol-gel process flow.

TABLE I. Two-factorial statistical designed screening experiment to initiate PZT sol-gel texturing study.

Name	Units	Type	Low actual	High actual
Pyrolysis temperature	°C	Numeric	250	350
Pyrolysis time	Minute	Numeric	1.5	4.5
Annealing temperature	°C	Numeric	650	750
Annealing time	Minute	Numeric	10	20

The lead sol comprises lead acetate trihydrate 99.99% diluted in 2-methoxymethanol 99.9% solvent. The lead sol was dehydrated at 100 °C for 2 hours. The zirconium + titanium sol (henceforth referred to as ZT) was created by first mixing Zr (IV) propoxide 70% in 1-proponal solvent (1-propanol 99%) at room temperature. After a few minutes of mixing, Ti (IV) propoxide 97% was added, mixed, followed by addition of acetyl acetonate, a chelating agent. The third sol was the hydrolysis sol comprising the de-ionized water (>18 Mohms) with 1-propanol 99% in equal ratios. After the lead sol has cooled down to room temperature, the ZT sol was added to it while stirring at 250 rpm. After one hour of stirring, the hydrolysis sol was added slowly and after four more hours of stirring, the clear sol was aged for 24 hours. The aged sol was then spun onto platinized silicon substrates ($Pt/Ti/SiO_2/Si$) at 3500 rpm for 30 sec. After spin coating, the thin films were pyrolyzed and annealed as per Table I below. Table I depicts a 2^4 full factorial screening

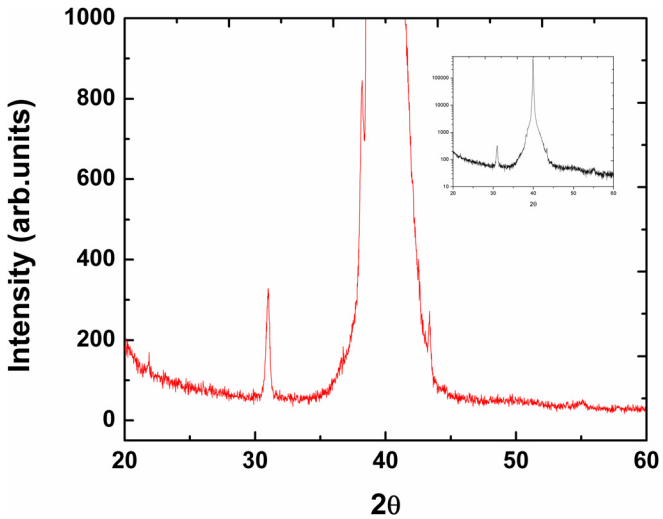

FIG. 2. (Color online) A typical XRD plot from a PZT sol-gel thin film showing small (100), substantial (110), and large (111) shoulder (inset shows the whole spectrum on log scale). The film was deposited on a platinized silicon substrate.

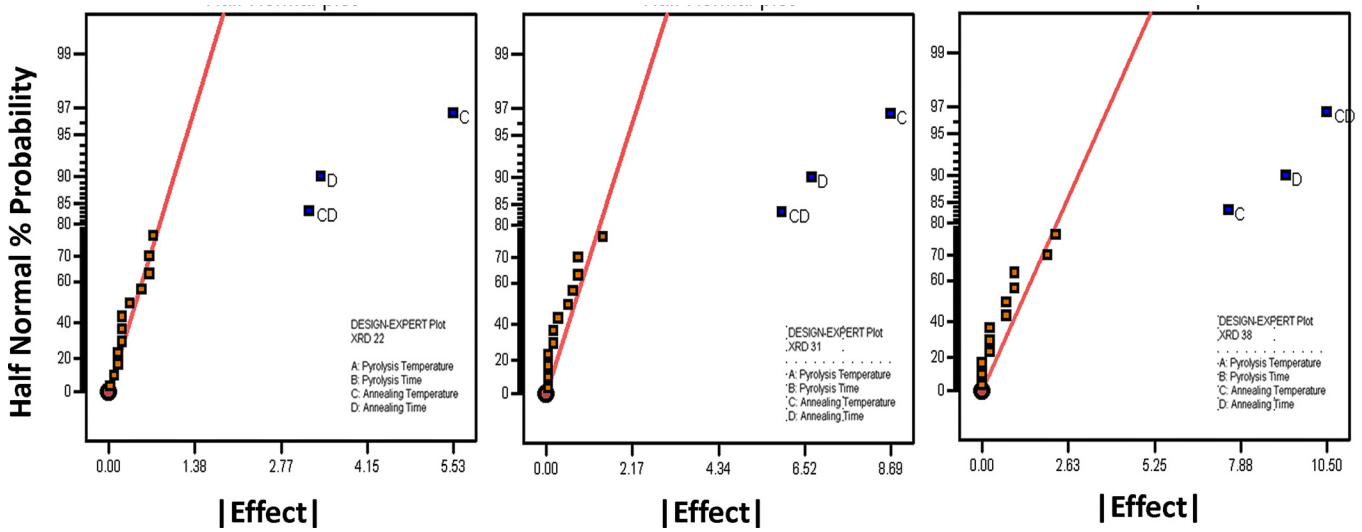

FIG. 3. (Color online) Half normal probability plots of XRD responses: (100), (110), and (111) peak heights.

experiment in the four factors (TCP)—pyrolysis time, pyrolysis temperature, annealing time, and annealing temperature. Pyrolysis was conducted on a hot plate while annealing was accomplished in a vertical furnace exposed to ambient air. The resultant thin film thickness was in the range of 65–85 nm.

The gelation process of pyrolysis and perovskite crystallization process of annealing were optimized for three different textures ((100), (110), and (111)) of PZT thin films on platinized silicon substrates. Subsequent detailed experimentation included the investigation on thermal budget to identify all the regions on operating space and the data from these samples were used to rigorously fill the TTT diagram for three different crystalline orientations. For the screening experiments, platinized silicon substrates from Nova Electronic Materials, FlowerMound, TX, were used and to develop the TTT diagrams followed by more detailed experiments, substrates from Inostek, Gyeonggi-do, South Korea, were utilized. The former had a micron of Pt over a Ti glue layer on SiO_2/Si while the latter had the configuration of 150 nm Pt/10 nm Ti/300 nm SiO_2/Si. X-ray diffraction was used to measure the orientation of the thin films. The X-ray peak heights (alternatively FWHM can be employed too) were measured and normalized. Design Expert software was used to generate and analyze the statistically designed screening experiments (SDE). JMP and R softwares were used in the mathematical modeling of the TTT data.

III. RESULTS AND DISCUSSION

A SDE of 17 (2^4+ 1 center point) runs was designed and conducted on the platinized Si substrates. These substrates had a micron thick Pt on Ti/SiO2/Si. XRD pattern was collected on 17 samples and the heights of peaks for (100) at $2\theta = 22°$, (110) at $2\theta = 31°$, and (111) at $2\theta = 38°$ was measured from the type of graph shown in Fig. 2. The normalized XRD peak heights for (100), (110), and (111) orientations were then used as the response of the SDE and an ANOVA (Analysis of Variance) was conducted. In the

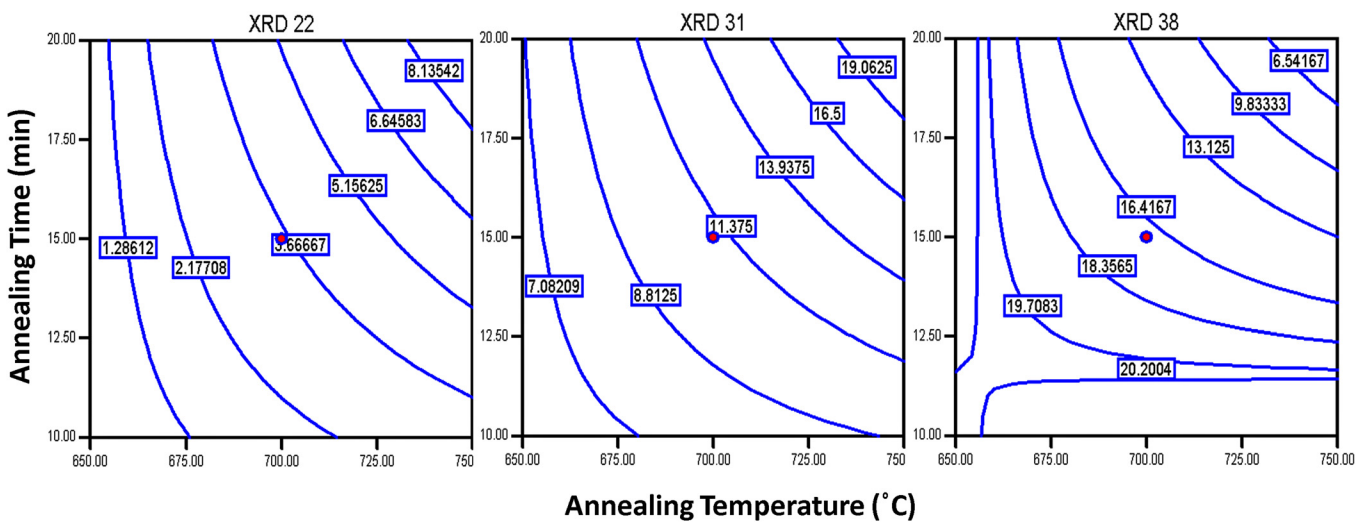

FIG. 4. (Color online) Contour plots showing increasing trends with respect to annealing conditions for (100) at $2\theta = 22°$, (110) at $2\theta = 31°$, and (111) at $2\theta = 38°$; the pyrolysis conditions were 300 °C and 3 min.

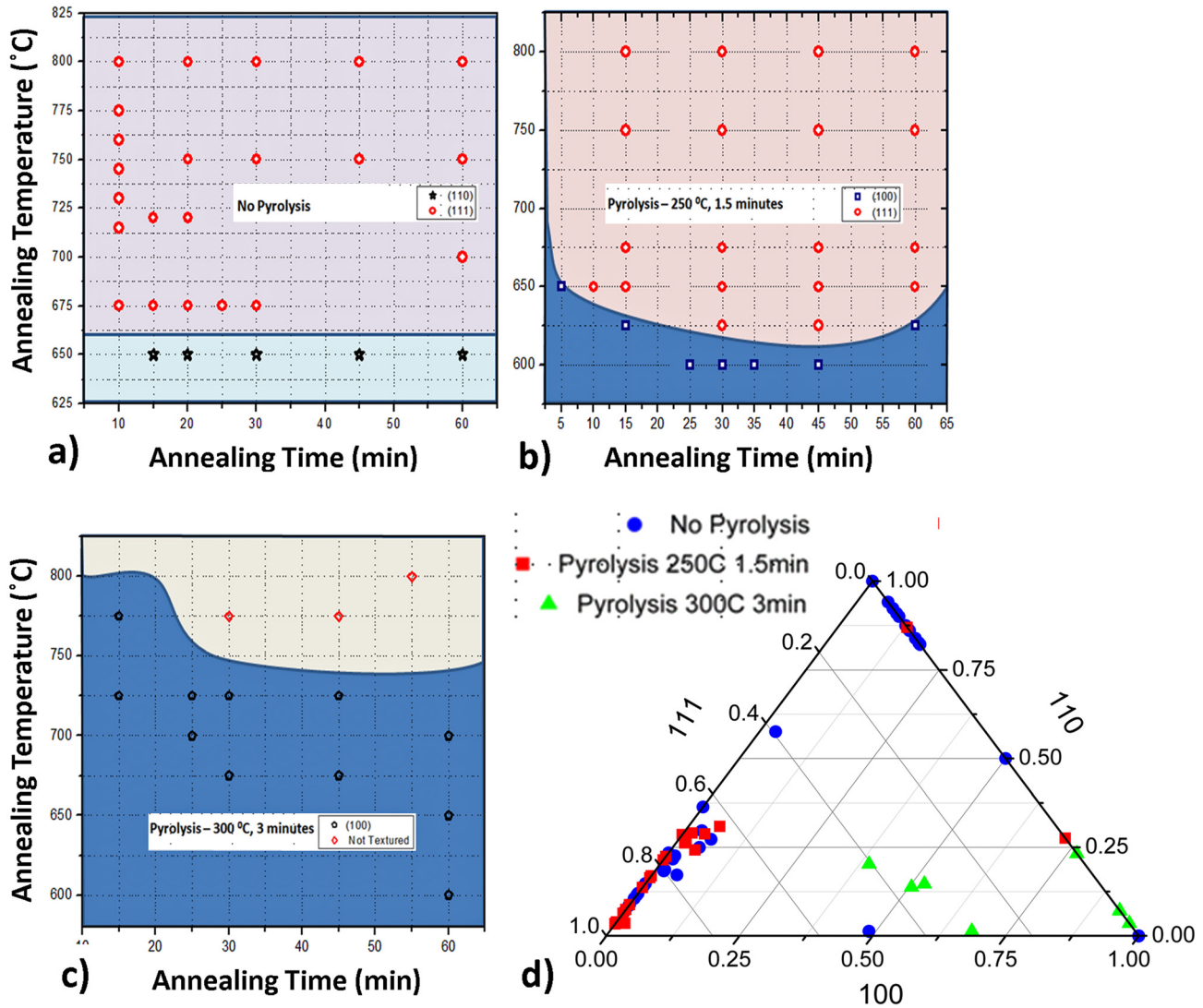

FIG. 5. (Color online) Temperature-time-transformation diagrams of PZT sol-gel thin films pyrolyzed at (a) no pyrolysis; (b) 250 °C, 1.5 min; (c) 300 °C, 3 min; and (d) the ternary plot of all the data.

experimental range explored, ANOVA shows that annealing temperature and time effects (C, D, and interaction CD) are more significant than the pyrolysis conditions (A, B, and interaction AB) and the interaction between the annealing and pyrolysis effects (AC, AD, BC, etc). This is clearly evident in the half normal probability plots of the Effects

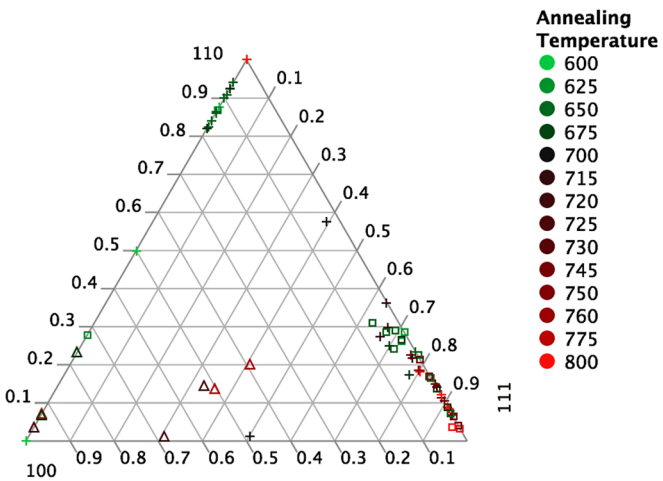

FIG. 6. (Color online) Observed data by pyrolysis coded by annealing temperature.

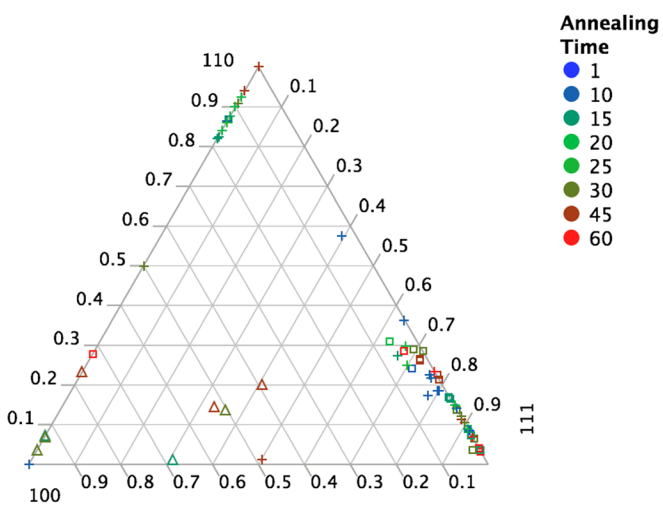

FIG. 7. (Color online) Observed data by pyrolysis coded by annealing time.

(measure of the process variable's influence on the response) shown in Fig. 3.

The resultant regression models generated the contour plots shown in Fig. 4. We find that higher annealing time and temperature yields higher desired peak (100) and decreases the undesired peak (111). However, the (110) peak also increases in this process regime. These XRD peaks were independent of pyrolysis time and temperature in the range explored. Also below 700 °C, longer annealing times will make the peak height independent of annealing time. Using this information, further extensive exploration of the sol-gel thermal budget operating space yielded the TTT diagrams shown in Fig. 5. This diagram is similar to that developed by Chen and Chen[8,9] except that their main process variables were pyrolysis temperature and time and they had maintained annealing temperature and time constant. It can be seen that films with pyrolysis at 300 °C for 3 min were textured in (100) direction until >750 °C annealing temperature, after which they start showing random orientation (labeled "not textured" in Fig. 5). This trend is a confirmation of the contour plot trends observed in the screening experiments. With an increase in annealing temperature and time, the (100) and (110) orientations increase while (111) orientation decreases and at >750 °C, all three orientation co-exist and so the film was not textured. On the other hand, the films pyrolyzed at lower

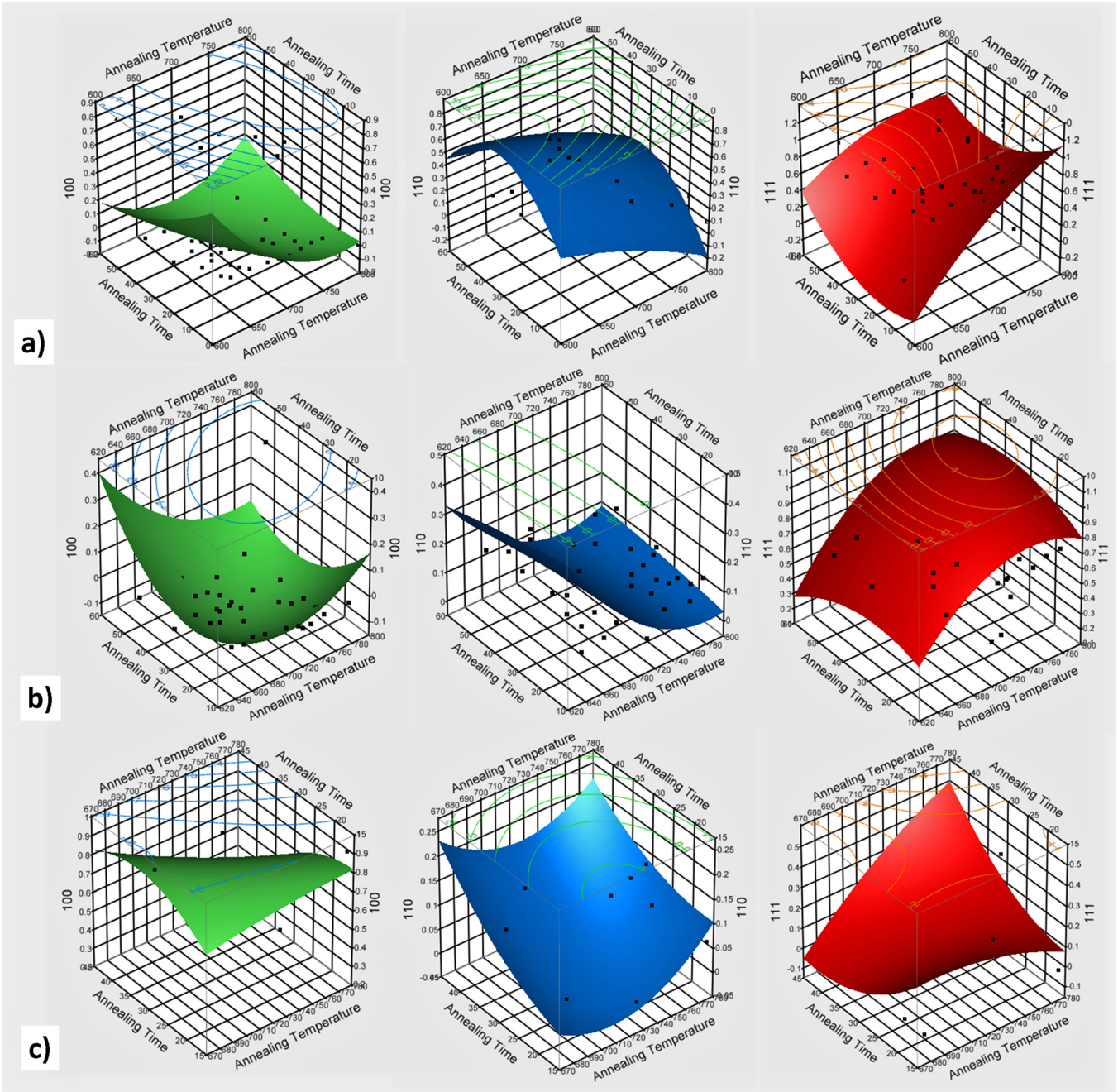

FIG. 8. (Color online) JMP contour plots of PZT sol-gel thin films pyrolyzed at (a) no pyrolysis: (100) with $R^2 = 0.662$, (110) with $R^2 = 0.381$, and (111) with $R^2 = 0.644$; (b) 250 °C, 1.5 min pyrolysis: (100) with $R^2 = 0.495$, (110) with $R^2 = 0.451$, and (111) with $R^2 = 0.527$; and at (c) 300 °C, 3 min pyrolysis: (100) with $R^2 = 0.722$, (110) with $R^2 = 0.961$, and (111) with $R^2 = 0.694$.

temperatures and for shorter times are textured in (100) or (110) (for no pyrolysis) direction until a certain threshold temperature and thereafter in (111) direction and that too is independent of annealing time. Ternary diagrams show the frequency of the orientations obtained for each pyrolysis binned as per the ranges in annealing temperature (Fig. 6) and annealing time (Fig. 7).

The data utilized to create the TTT diagrams were analyzed using the JMP statistical software and the quadratic fits are shown in Fig. 8. Despite moderate R^2 values (reported in the figure description), the predictability of the quadratic models was found to be poor. A good hint toward this unpredictability can be witnessed in the portion of points that do not trend with the surface plots. We omitted to include the proportionality between the crystalline orientations (the three box plots at the apex of Fig. 9), which can explain this difference. In the left bottom of this figure, one can also notice the large spread in the response data (i.e., the lack of a linear or higher order trend) with respect to the processing variables.

Multiple regression takes a single response (or several separately one at a time) and models its relationship to multiple independent factors. The quadratic model, which is a multiple regression, was inadequate to explain correlated response data evocative of XRD pattern data. To model this joint relationship, a multivariate regression approach had to be employed. Multivariate regression simultaneously relates several responses to each other and to multiple independent factors. As mentioned earlier, the XRD peak data was normalized and so the three responses add up to one and therefore are inherently related (i.e., not independent). Therefore, we must model them simultaneously. As pyrolysis conditions were lumped into three pairs of temperature and time combinations in the TTT experimentation, each pair was considered as a single categorical process variable. The other two process variables were considered as either categorical or continuous variable in the regression.

After separate independent regressions (the aforementioned quadratic regression), two other methods of regression, multinomial logistic,[12] and log ratio multivariate,[13] were evaluated. For multinomial regression, we convert the normalized XRD data into counts. Bearing in mind that the normalized data are the observed proportions of crystalline orientations in each film or sample, then the 100 points or counts can be the sum total of all three crystalline orientations. For example, if we observed percentages of 5%, 10%, and 85%, we would assign counts of 5, 10, and 85, respectively. Now we treat this transformed data as observed counts from a multivariate binomial (multinomial) distribution. Our multinomial distribution is described by three parameters representing the true unordered proportions in our mixture: p[100]; p[110]; p[111] with $p[100]+p[110]+p[111]=1$. In order to perform regression to model these parameters we use Eq. (1) below

$$Lin[100] = \ln\left(\frac{p[100]}{p[111]}\right) = X\alpha,$$
$$Lin[110] = \ln\left(\frac{p[110]}{p[111]}\right) = X\beta, \tag{1}$$

where X is the covariate matrix from pyrolysis, annealing time, and annealing temperature, α and β are the regression coefficients that we estimated using maximum likelihood methods. Together $X\alpha$ and $X\beta$ are called linear predictors. After modeling Lin[100] and Lin[110], p[100], p[110], and p[111] can be recovered from Eq. (2):

$$p_{[100]} = (1+\exp(-Lin[100])+\exp(Lin[110]-Lin[100]))^{-1},$$
$$p_{[110]} = (1+\exp(-Lin[110])+\exp(Lin[100]-Lin[110]))^{-1},$$
$$p_{[111]} = (1+\exp(Lin[100])+\exp(Lin[110]))^{-1}. \tag{2}$$

The main concept here is that the data are counts from a multinomial distribution and the unknown parameters are proportions. The linear predictors are the ratio of probabilities of occurrence of each orientation in a particular thin film sample at the stipulated thermal conditions. The second method evaluated was log ratio regression for which multivariate normal regression of the log of the ratios of the normalized XRD peak data was performed. As in the multinomial case, this method also preserves the constraint that the data must sum to one. The log ratio strategy as described by Aitchison[13] transforms similar to that in multinomial regression. For the log ratio technique, we transform the data (100), (110), and (111) through Eq. (3):

$$LR1 = \ln\left(\frac{[100]}{[111]}\right),$$
$$\mathrm{LR2} = \ln\left(\frac{[110]}{[111]}\right). \tag{3}$$

Thus the new data are LR1 and LR2 with mean vector ($\mu 1$; $\mu 2$) and covariance matrix S. In order to perform regression we use Eq. (4):

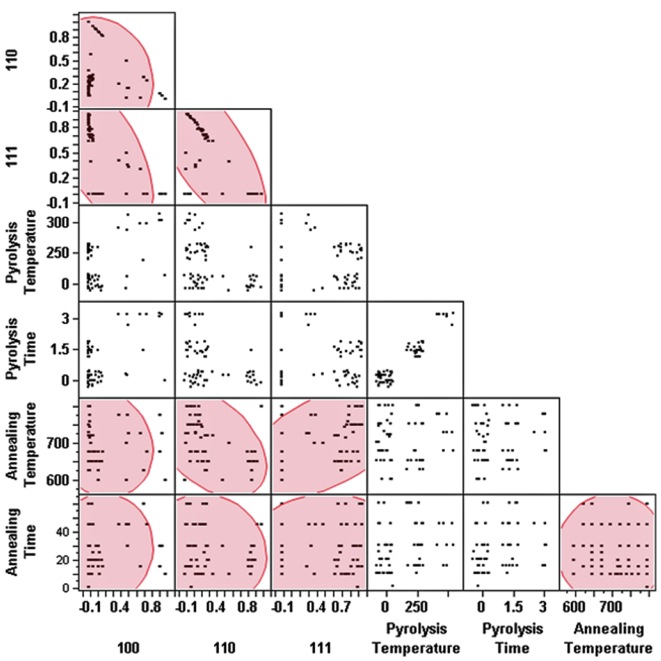

FIG. 9. (Color online) JMP scatterplot matrix of the responses (XRD peak data) vs the factors: pyrolysis and annealing conditions.

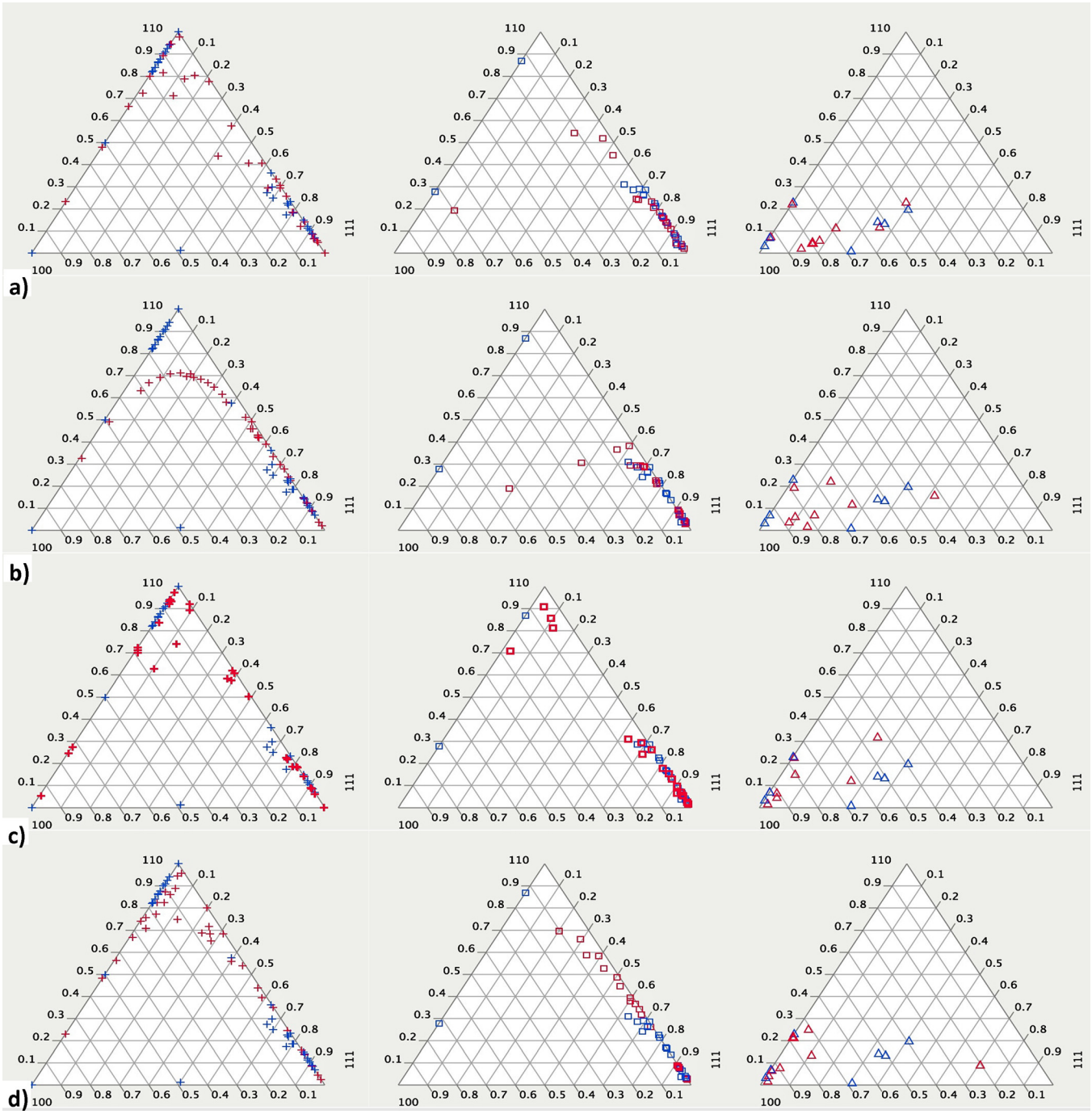

FIG. 10. (Color online) Actual vs predicted for (a) multinomial categorical, (b) multinomial continuous, (c) log-ratio categorical, and (d) log-ratio continuous (blue-observed, red-fitted) models.

$$\begin{aligned} \mu_1 &= \mathrm{X}\alpha, \\ \mu_2 &= \mathrm{X}\beta. \end{aligned} \tag{4}$$

After modeling $\mu 1$ and $\mu 2$, we can recover the fitted (predicted) concentrations with Eq. (5):

$$\begin{aligned} [\widehat{100}] &= (1 + \exp(-LR1) + \exp(LR2 - LR1))^{-1}, \\ [\widehat{100}] &= (1 + \exp(-LR2) + \exp(LR1 - LR2))^{-1}, \\ [\widehat{100}] &= (1 + \exp(LR1) + \exp(LR2))^{-1}. \end{aligned} \tag{5}$$

Therefore, in this case, the main concept is that the data are in LR1 and LR2, and they are normally distributed with parameters mean and covariance matrix.

The purpose of regression is to find α and β so that $\mathrm{X}\alpha$ and $\mathrm{X}\beta$ best describe or fit the data. Both the multinomial and the log-ratio regression will produce estimates for α and β. The columns of the X matrix can be either categorical or continuous predictors. Categorical variables such as "High", "Medium", "Low", or "Red", "Green", "Blue" describe distinct states of classes. Continuous variables such as "Length",

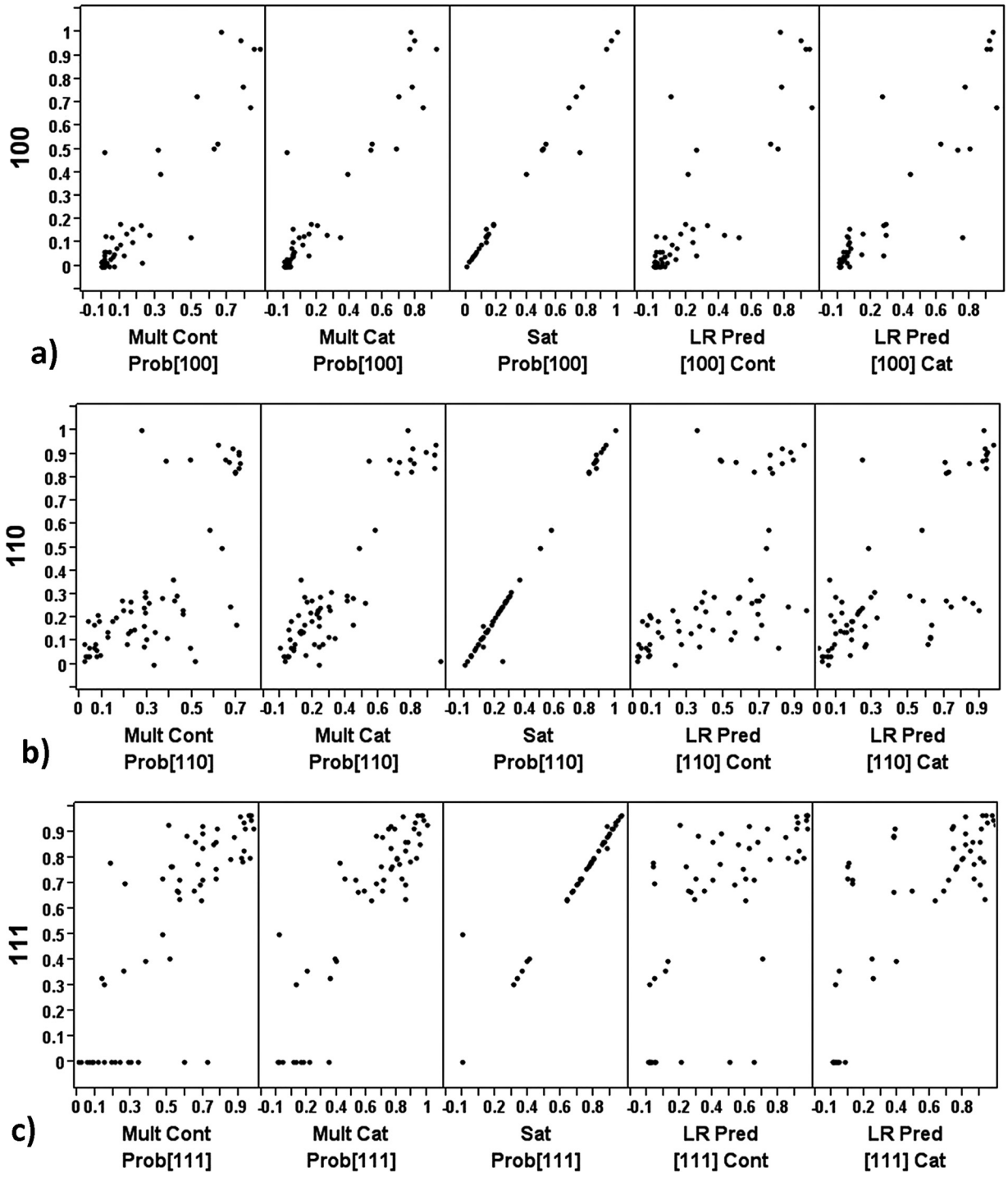

FIG. 11. Actual vs fitted for (a) (100), (b) ([110), and (c) (111).

"Age", and "Weight" are measured on a continuous scale. Often when we have continuous regressors such as temperature, we can either use continuous values or discretize them by binning them into categories such as "High", "Medium", and "Low". The benefit of using continuous regressors over categories is reduction in the number of terms, which means savings in efficiency or fewer samples needed for good model fitting. The benefit of using categories is that they are more flexible and tend to fit better when a non-linear relationship exists. As mentioned previously, we will always use pyrolysis as a categorical variable with three settings. Annealing time and temperature can be used as either continuous or categorical variables, so we will fit both continuous and categorical models and compare their characteristics.

In the continuous model, we will use pyrolysis "P" (P1, P2, P3) as a categorical variable and annealing time (Tm) and annealing temperature (Tp) as continuous variables. Our linear predictors $X\alpha$ and $X\beta$ are now

TABLE II. XRD normalized data vs. model predictions for four different samples.

Sample	Pyrolysis and annealing conditions	XRD peak	Actual	Multinomial categorical model	Multinomial continuous model	Log-ratio categorical model	Log-ratio continuous model
SG1	300 °C, 3 min	(100)	0.88	0.924	0.878	0.928	0.952
	675 °C, 30 min	(110)	0.12	0.076	0.0417	0.0721	0.0428
		(111)	0	4.29×10^{-6}	0.08	0.0003	0.0056
SG2	300 °C, 3 min	(100)	0.896	0.924	0.878	0.928	0.952
	675 °C, 30 min	(110)	0.104	0.076	0.0417	0.0721	0.0428
		(111)	0	4.29×10^{-6}	0.08	0.0003	0.0056
RV1	300 °C, 3 min	(100)	0.91	0.924	0.878	0.928	0.952
	675 °C, 30 min	(110)	0.09	0.076	0.0417	0.0721	0.0428
		(111)	0	4.29×10^{-6}	0.08	0.0003	0.0056
RV2	250 °C, 1.5 min	(100)	0.0042	0	0	0.0008	0.0007
	800 °C, 30 min	(110)	0.083	0.022	0.034	0.0172	0.0273
		(111)	0.875	0.978	0.966	0.982	0.972

$$\begin{aligned} X\alpha &= \alpha_0 + \alpha_p P + \alpha_{Tm} Tm + \alpha_{p*Tm} P*Tm + \alpha_{p*Tp} P*Tp + \alpha_{Tp} Tp \\ &\quad + \alpha_{Tm*Tp} Tm*Tp + \alpha_{p*Tm*Tp} P*Tm*Tp, \\ X\beta &= \beta_0 + \beta_p P + \beta_{Tm} Tm + \beta_{p*Tm} P*Tm + \beta_{p*Tp} P*Tp + \beta_{Tp} Tp \\ &\quad + \beta_{Tm*Tp} Tm*Tp + \beta_{p*Tm*Tp} P*Tm*Tp. \end{aligned} \quad (6)$$

Notice that "P" and all α's and β's associated with "P" change depending on whether P = P1, P2, and P3. Since pyrolysis (P) can take on three values, we are fitting three models at the same time.

$$\begin{aligned} X\alpha &= \alpha_0 + \alpha_p P + \alpha_{Tm} Tm + \alpha_{p*Tm} P*Tm + \alpha_{p*Tp} P*Tp + \alpha_{Tp} Tp, \\ X\beta &= \beta_0 + \beta_p P + \beta_{Tm} Tm + \beta_{p*Tm} P*Tm + \beta_{p*Tp} P*Tp + \beta_{Tp} Tp. \end{aligned} \quad (7)$$

In the categorical model we treat Tm and Tp as categories. Our linear predictors' form remains the same but there are fewer interaction terms (Eq. ((7)). In this case, we fit a separate model for each P, Tm, and Tp combination. If we had five levels of Tm, five levels of Tp, and three levels for P, we would have 75 models that we estimate at the same time.

We used continuous and categorical models of both the multinomial and the log ratio methods to fit the data. We then compared them to the observed data and the saturated categorical model (which is essentially the same or a point by point fit). From Figs. 10(a)–10(d) we see that the categorical models have better fits than the continuous ones, suggesting a possible nonlinear relationship in the predictor. Also, it seems that the multinomial model has a better fit than the log ratio model. This is confirmed when plotting observed versus fitted data for each (100), (110), (111) orientations separately in Figs. 11(a)–11(c). Besides the saturated model, which is not a realistic model (unless we have replicates), the categorical model with the multinomial data (second from the left) gives the closest fit to the one-to-one line for the observed and fitted values.

In using the multinomial model with categorical factors for prediction, the choice of annealing temperature and time is restricted to that used in the original model while with continuous factors, any annealing temperature and time value (but within the range used in the model) is permitted. To elucidate (refer to Figs. 6 and 7), with the continuous model one can predict the response for an annealing temperature of 685 °C and 22 min but for the categorical model (where discretized fixed values of the factors are used), we have to use an annealing temperature and time that have been used in the original regression (say, 675 °C or 700 °C and 20 or 25 min but not necessarily the same original combination of the two factors).

For final experimental verification, we created four samples, SG1, SG2, RV1, and RV2 (Table II), where SG and RV refers to PZT sol created up by two different operators but SG1, SG2, and RV1 were processed at the same pyrolysis and annealing condition. From Fig. 12, we see that the predictability using multinomial categorical fit is the best among the four models attempted. The continuous models over predict the lowest rank response (i.e., they are not very good at predicting a zero response). The log ratio models consistently over predict the predominant orientation (i.e., the largest response). Based on these results, we believe this mathematical formulation of TTT diagram allows the prediction of the predominant orientation and the ranking of each orientation of interest (i.e., the orientations used in the XRD data modeling). This regressive modeling can be applied to

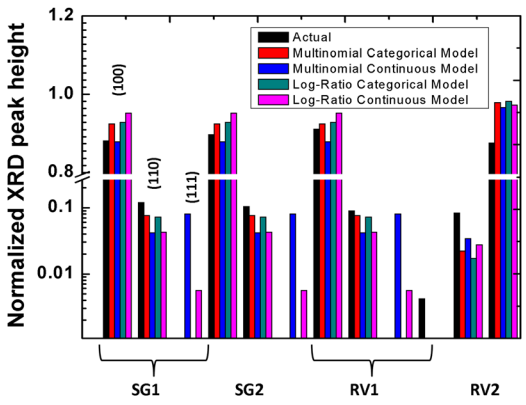

FIG. 12. (Color online) Comparison of prediction results for four sol-gel samples shown in Table I.

more than three peaks of an XRD pattern and therefore, for "n" number of peaks will lead to "n" proportions and (n-1) equations similar to Eq. (1). In addition, such a type of modeling can be undertaken for XRD patterns from any (i.e., non-PZT) thin film or bulk ceramics (including PZT). Understandably, this mathematical approach is only as accurate as the methodology employed in calculating the XRD peak heights.

IV. CONCLUSIONS

In summary, we developed a mathematical model to refine the typical temperature-time-transformation (TTT) diagrams by quantitatively describing both the predominant phase and any secondary phases. Utilizing data from the two-step thermal treatments (pyrolysis and annealing) of a PZT sol-gel or chemical solution deposition process, different regression schemes, namely, multiple linear, multinomial, and multivariate, were explored to derive predictor models for the level of (100), (110), and (111) crystallinity in a thin film sample. The best validation of experimental data was obtained with multinomial regression. We have demonstrated the simplicity and efficacy of this methodology for every day laboratory use and expect extendibility to non-thin film systems. In doing so, we have also taken out some of the specificity, like operator-induced variability, that is usually observed in such experimentation.

ACKNOWLEDGMENTS

The authors gratefully acknowledge financial support from the Air Force Office of Scientific Research (AFOSR), and Institute for Critical Technologies and Applied Science (ICTAS).

[1]J. Kuwata, K. Uchino, and S. Nomura, Ferroelect. **37**, 579 (1981).
[2]J. Kuwata, K. Uchino, and S. Nomura, Jpn. J. Appl. Phys. **21**, 1298 (1982).
[3]S.-E. Park and T. R. Shrout, J. Appl. Phys. **82**, 1804 (1997).
[4]S.-E. Park and T. R. Shrout, IEEE Trans. Ultrason. Ferroelect. Freq. Contr. **44**, 1140 (1997).
[5]H. Fu and R. E. Cohen, Nature (London) **403**, 281 (2000).
[6]X.-H. Du, J. Zheng, U. Belegundu, and K. Uchino, Appl. Phys. Lett. **72**, 2421 (1998).
[7]G. J. Norga and L. Fe, Mater. Res. Soc. Symp. Proc. **655**, CC9.1.1 (2001).
[8]S.-Y. Chen and I-W. Chen, J. Amer. Ceram. Soc. **77**, 2337 (1994).
[9]S.-Y. Chen and I-W. Chen, J. Amer. Ceram. Soc. **77**, 2332 (1994).
[10]Z. Huang, Q. Zhang, and R.W. Whatmore, J. Mater. Sci. Lett. **17**, 1157 (1998).
[11]C.-S. Park, S.-W. Kim, G.-T. Park, J.-J. Choi, and H.-E. Kim, J. Mater. Res. **20**, 243 (2005).
[12]A. Agresti, *Categorical Data Analysis* (Wiley-Interscience, New York, 2002).
[13]J. Aitchison, *The Statistical Analysis of Compositional Data (Monographs on Statistics and Applied Probability)* (Springer, New York, 1986).